FINITE ELEMENT MODELING OF COMPOSITE PLATES CRUSHING USING IMPLICIT AND EXPLICIT INTEGRATION SCHEMES

Alexandre Muniz Neves, alexandre.muniz.neves@gmail.com
Flávio Luiz de Silva Bussamra, flaviobu@ita.br
Eliseu Lucena Neto, eliseu@ita.br
Instituto Tecnológico de Aeronáutica, Praça Marechal Eduardo Gomes, 50 – Vila das Acácias CEP 12228-900 – São José dos Campos –SP – Brasil

Abstract. *The difficulty in predicting the failure mechanics when a laminate composite plate suffers an impact is a challenge in the project of impact-resistant composite structures. The objective of this work is to contribute in identifying these mechanics by means of finite element models capable of representing failure modes in carbon fiber specimens under dynamic compression. This study followed an extensive test campaign, which is explained in detail. The models are solved by direct time integration, using both implicit and explicit schemes. Numerical results are then compared with experimental data.*

Keywords*: finite element modeling, dynamic loading, crushing of plates.*

1 – INTRODUCTION

It is fundamental, in a variety of situations, to predict the crashworthiness of a composite structure. To achieve this goal, it is necessary to define what the mechanics of energy absorption are, how efficient are they and how the damage evolves within the structure of the laminate in a way to absorb the kinetic energy.

Composite materials, unlike metals, present no significant plastic behavior due to the typically brittle nature of most of the fibers. Even so, works by Mammalis et al. (1997) and Silvestre (2005) show that composite materials can still have a reasonable capacity to absorb energy in an impact. This is thanks to the appearance of multiple damages on the material, which creates a progressive fragmentation/delamination pattern, which yields a kind of "average plasticity" behavior, capable of absorbing large quantities of energy. There are already structures which are designed specifically to this purpose, like the noses of Formula 1 cars.

With the tools available today, however, the design of a high performance energy absorbing structure is somewhat complex and time-consuming, due to the need to evaluate, with reasonable trust, the mechanics of failure. This is still a difficult task, especially when we have to analyze a complex impact condition.

To make the design and optimization of these kinds of structures plausible, since its conception until the final product, it is mandatory to develop calculation methods that are efficient in the prediction of the failure behavior of these materials. If this is successfully done, the industry will be able to design structures based not only in their capacity to sustain the workloads expected in normal operation, but also in their capacity to sustain damage, without having to rely solely on qualification tests.

In this study, a commercial code based in the method of finite elements is used. The chosen tool was the Belgian software named Samcef (*Système pour l'Analyse des Milieux Continus par Eléments Finis*).

The development of the finite element models is based on the results obtained in the experiments conducted recently by Guillon (2008). The numerical model developed focuses on improving the understanding of the failure mechanics in a qualitative and quantitative way, so as to enrich the experimental analysis and build the way for future studies in the area.

2 – THE EXPERIMENTAL CAMPAIGN

The experimental campaign consisted on the compression of carbon fibre reinforced plastic plates. The tests were performed with a multitude of different layups and geometries. Dynamic crushing (free fall from a predetermined height) and quasi static crushing (driven slowly by a test machine) tests were performed, and the results of force and displacement collected together with videos from high-speed cameras. The campaign is explained below in detail.

2.1 – The Experimental Apparatus

2.1.1 - Stabilizing Assembly

To stabilize the impact of the specimens and avoid global buckling (which would lead to an unstable crushing) a stabilizing assembly was designed. The assembly stabilizes the plate over all its length with two vertical bars resting at a distance of 0.1 mm of the two faces of the plate. Close to the contact area, the assembly leaves a free distance to the impact base, with two horizontal bars, screwed to the vertical ones, supporting the plate laterally. This configuration

creates virtually bi-dimensional boundary condition at the region of the contact between the plate and the rigid base, so to allow the failure to develop almost uniformly over the whole width of the plate.

The assembly is composed of:

- 4 vertical bars stabilizing the plate length-wise, to prevent buckling;
- 2 horizontal bars, supporting the plate width-wise, assuring quasi-uniform behaviour in this direction;
- 4 vertical and 2 horizontal supports, to adjust the position of the bars;
- two mounts to fix the assembly in place;
- an impact base made of machined high-carbon steel, modified according to the needs of each test.

The final piece to complete the assembly is the metal cylinder that holds the specimen, and also serves as the physical mean for the introduction of efforts. Attached to the cylinder there is a piezo-electric load cell that measures the efforts on the plate.

This assembly can hold a plate of 120 x 60 mm. The thickness of the specimens can vary from 0 to 10 mm and the free height can be adjusted between 0 and 40 mm. The scheme of the assembly is shown in Fig. 2.1.

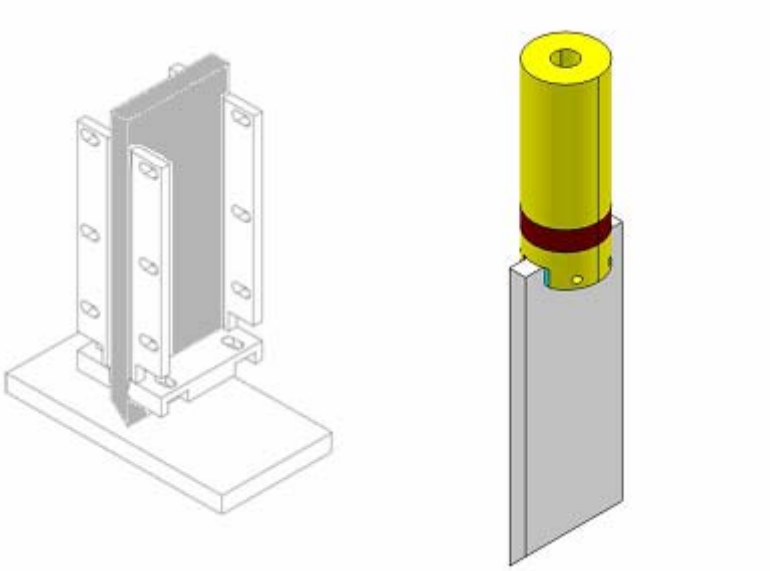

Figure 2.1. The specimen mounted on the stabilizing assembly (left) and the specimen fixed on the cylinder containing the load cell (right).

2.1.2 – The machine for quasi static tests

The quasi-static tests were run in a universal "INSTRON" machine for mechanical tests, with 100 kN capacity. The tests consisted on the forced displacement of the specimen, fixed to the machine axis, that moves impelled by a screw.

2.1.3 – The drop tower for dynamic tests

The assembly is also mounted on the drop tower for the dynamic tests. The tower is equipped with a car, whose weight can vary from 36 to 205 Kg, which can be released from a maximum height of 5 m.

2.1.4 – Instrumentation

All the signals are registered with an oscilloscope (brand Yokogawa 708D), so the curve force *x* displacement can be saved and analyzed *a posteriori*. For the quasi-static tests, the machine is already instrumented to measure displacements and efforts. For the tests on the tower, the efforts were measured by a load cell, placed on the cylinder that holds the specimen. One accelerometer is placed in the car, allowing us to obtain redundant effort measurements. The displacement is calculated by integrating the acceleration in time twice. The initial condition for this integration procedure is the speed of the car just before the impact. This speed is measured by an optic sensor.

All the tests were recorded by a high-speed digital camera, in a maximum frequency of 20000 images per second, so, for the sake of redundancy, the development of the test and the initiation of the various relevant modes of damage can be carefully observed.

2.2 – The specimens

2.2.1 – Geometry

In all the tests, the geometry of the specimens was a flat plate. The face of the plate that impacts the solid base is machined in a particular geometry in order to favour one specific failure mode. The geometry of the impacting face is called the "trigger".

Three models of triggers were used in the campaigns, and two of them were modeled, as follows:

1 – Point (PO) – The face of the plate that impacts the base was machined flat, perpendicular to the other two. The impact base was a machined point that impacts the laminate in the middle and divides it in two branches

2 – Chamfer (CH) – A chamfer at 45 degrees is machined in the side of the plate that impacts the base, which is flat.

The geometry of the triggers is drawn in detail in Fig. 2.2.

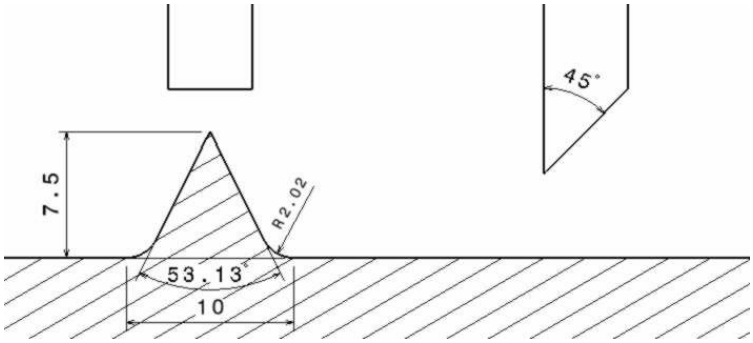

Figure 2.2. The two different triggers used in the tests.

2.2.2 - Materials and lay-ups

Four campaigns were conducted in total, each with a different type of lay-up. Only one of those was modeled in finite elements. For this campaign, described next, specimens made in industrially controlled conditions were used.

The specimens consisted of plates of 160mm x 60mm, composed by 20 or 32 plies of unidirectional, pre-impregnated carbon/epoxy HexPly Unidirectional/M21/35% (resin mass fraction)/268g/m^2 (weight of the plies)/T700GC. These were fabricated by EADS.

Two lay-ups were tested:

1 – (UDFoG) $[(0/45/90/135/0)_2]$s (20 plies, thickness of 5.2 mm, specific mass of 1535 Kg/m^3)

2 – (UDISOFoG) $[(45/0/-45/90)_4]$s (32 plies, thickness of 8.3 mm, specific mass of 1575 Kg/m^3)

In all these tests the free height of the stabilizing assembly was fixed in 20 mm.

The standard direction for the orientation of the material was the direction of the crushing of the plate. So 0 degree means that the fibers are aligned perpendicularly to the surface of impact.

Table 2.1 shows the number of tests conducted for each lay-up type and each one of the triggers.

Table 2.1. Crushing tests.

Material Layup	Speed	Trigger		Number of tests
		Chamfer	Point	
(UDFoG)				13
$[(0/45/90/135/0)_2]$	QS	5	1	6
	DYNA	3	1	4
$[(45/0/-45/90)_4]$s	QS	2	0	2
	DYNA	1	0	1

2.3 – The procedures

In the quasi-static tests (called QS), the speed of the displacement imposed by the machine was 200 mm/min. In the dynamic tests (called DYNA), made on the drop tower, the initial height was always 1.5 m, which resulted in a speed of impact a little over 5 m/s. The weight of the car varied from test to test (36, 72 or 106 Kg), and was adjusted in order to produce only the amount of energy needed to crush each plate until the end of its length, without unnecessarily damaging the surface of the base or the instrumentation.

The free height left between the horizontal stabilizing bars and the base was fixed for each test, and adjusted so to allow the formation of a progressive crushing front with a desired fail mode, and still keep the delamination as uniform as possible in the direction of the width. The height was fixed in 20 mm for the numerical models.

3 –THE FINITE ELEMENT MODELS

3.1 – General aspects and objective of the model

The damage and rupture of a composite material usually result from a number of different microscopic mechanisms. Obviously a microscopic approach is impractical in a finite element analysis of a structure. We can, however, build a model capable of predicting some of the material behaviors in a laminate level. At this level, we can model the damage as a result of three different, but coupled phenomena: the matrix failure, the fiber failure and the delamination.

To access these modes of failure we had to build a model that represented each ply and each interface between plies accurately. Therefore, each ply of the laminate had one element across its thickness, and also each layer of resin between two plies had one element in its thickness. In order to reduce the size of the model, the width of the plate was reduced from 60 mm to 0.25 mm (represented by one element only in the width direction) so only a small section of the specimen was represented. Its length was also reduced from 160 mm to 100 mm, since after 50 mm of crushing all the specimens present an almost flat force x displacement curve.

3.2 – Geometry and mesh

The bulk file containing the model was written in plain text file, and the geometry and mesh of the model, in a parametric manner, so that they could be manipulated easily. With the geometry and solution parameters data input from the user, the mesh and boundary conditions are automatically generated by the code.

Two models were built, each with two loading cases (dynamic and quasi-static) representing the crushing of the plates with point and chamfer triggers, using 3D elements.

The final model was supposed to represent the specimens used in the UDFoG campaign. Therefore, they had a thickness of 5.2 mm and were made of 20 plies of unidirectional carbon, aligned in 0, 90 and 45 degrees angles.

For the final models, the height of the plate was 100 mm, the free distance between the stabilizing assembly and the base was 20 mm and the free distance between the stabilizing assembly and the lateral faces of the plate was 0.1mm.

All the interface elements modeled had a standard thickness of 0.02 mm. The final point trigger and chamfer trigger models had 35,214 and 34,146 nodes, respectively.

The global coordinate system was defined as shown in Fig. 3.1: x (DOF 1) in the direction of the thickness of the plate, y (DOF 2) in the direction of the height of the plate, and z (DOF 3) in the direction of the width of the plate.

Figure 3.1 shows a perspective view of the point trigger full-size model.

Figure 3.1. Perspective view of the full-sized point trigger model.

3.3 Boundary and initial conditions

For the dynamic simulations, concentrated mass elements were assigned to the topmost nodes of the plate, to represent the weight of the car used in the drop tower. The mass assigned to each node was the total mass of the car (106 Kg) divided by the number of nodes and multiplied by the ratio between the model width and the real width of the plate (60 mm). Moreover, an initial velocity of -5m/s and an acceleration of -9.81 m/s^2, on component 2, were imposed on all the nodes of the plate, to represent the kinetic energy of the falling car in the moment of impact and the body forces.

For the quasi-static models, a forced displacement of 5mm/s was imposed on the nodes on the top of the plate, so that their displacement would force the crushing of the plate against the base. On these models the inertia forces were disregarded.

In both models the nodes of the top of the plate had their translation degrees of freedom restrained in components 1 and 3, so they could only translate in the crushing direction. All the nodes of the plate had their component 3 restrained, so that they could not move out of the plane defined by the direction of crushing and the normal to the plate face.

The stabilizing assembly was modeled with meshed 3D elastic elements. The nodes of the face of the base opposite to the face where the plate crashes had all their DOF fixed, as were the nodes of the assembly face opposite to the plate. The sums of forces in the stabilizing assembly and in the impact base were collected as outputs, to be later compared with experimental values.

3.4 Materials

The material of the base was modeled as a linearly elastic. Since it was of no interest to evaluate stresses on the base, approximate mechanical properties of high-carbon steel were adopted.

The constitutive functions used for the carbon fiber plies and interfaces were modeled much more carefully, since they were the object of interest in the analysis. Both were given non-linear laws with the possibility of damage. The laws and hypotheses are described below.

The mechanical properties of the carbon fibre were extracted from tests made described by Pinho et al. (2004). The elastic modules and the rupture limits were defined by five tests: traction at 0 degrees, compression at 0 degrees, compression at 90 degrees, traction at +/-45 degrees and traction at +/-67.5 degrees.

The surface energy release associated to the damage has been defined based on the matrix failure modes, through evaluation of the energy dissipation in interface opening (G_I and G_{II}) tests. The mechanical properties used in the model are presented in Tab. 3.1.

Table 3.1. Carbon/epoxy material mechanical properties

E_1 (MPa)	E_2 (MPa)	G_{12} (MPa)	ν_{12}	
125000	9000	5000	0,4	
X_t (MPa)	X_c (MPa)	Y_t (MPa)	Y_c (MPa)	S_c (MPa)
1950	1950	75	220	150
$G_{\text{fibre traction}}$	$G_{\text{fibre comp}}$	G_I (mJ/mm^2)	G_{II} (mJ/mm^2)	
133	80	0.35	1.2	

Where X_t and X_c are the rupture stresses in traction and compression in the direction of the fiber, and Y_t and Y_c, the corresponding stresses for the direction perpendicular to the fiber. Sc is the rupture stress in plane shear, and G_{xx} are the energies dissipated in the various failure modes.

The test in traction at 45 degrees shows that the material presents a plastic behavior in shear. The curve stress x strain is only linear until we reach stresses close to 75 MPa. After this point, the rigidity falls continuously until the rupture, which occurs at a stress of 150 MPa. The shear strain in the point of rupture reaches 15%. This plastic behavior is taken into account in the material properties definition.

The carbon plies were modeled with a non-linear elastic material subject to damage, called “Dual” in Samcef. It consists of a material whose loading and curve can be defined by the user in terms of functions relating the stress and strain in traction, compression and shear. Therefore, it can model an anisotropic material whose behavior is particular in traction, compression and shear.

The inputs from the user are the stress-strain curve before rupture (linear or non-linear), the strain where the degradation starts and the strain where rupture occurs, that is, where the material has zero stress no matter its deformation and is deleted from the model. The loading and unloading paths of this element are exemplified in Fig. 3.2.

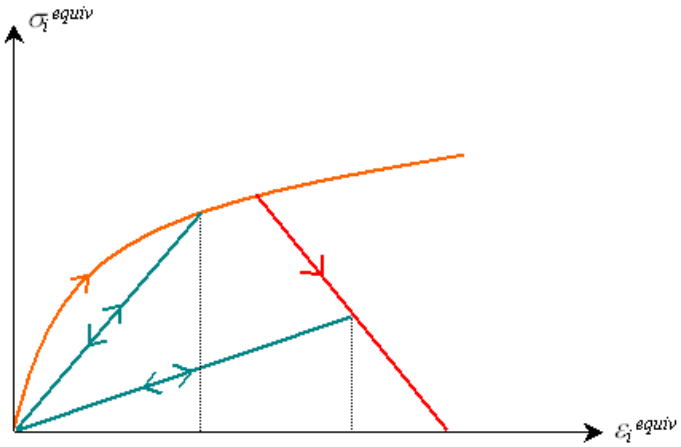

Figure 3.2. Load and unload paths for the material law "dual".

Figure 3.3 shows the function used to define the elastic-plastic behaviour of the carbon fibre in xy-shear.

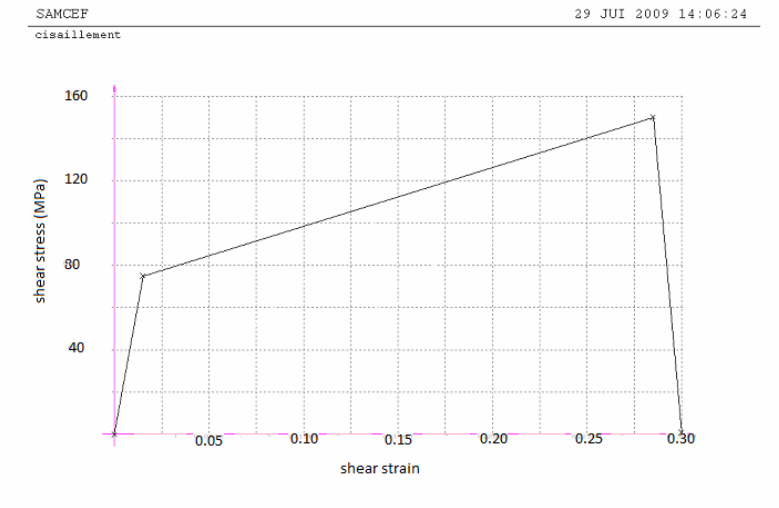

Figure 3.3. Material behavior in shear.

3.5 – Interfaces

Samcef uses a specific element hypothesis to represent the interfaces between plies of composite structures. It represents physically a homogeneous resin layer that transfers the stresses between the plies, up to a maximum allowable deformation.

In the post-processing, it gives results of inter-laminar stresses (peel as component 3 and transverse shear as components 5 and 6 for the shear planes 12 and 23 respectively) and scalar damage.

Various damage models, according to the material chosen, can be associated to the interface element in order to simulate delamination damage phenomena. The damage model chosen for the implicit solution model was the Smith-Ferrante cohesive law, widely used for fracture mechanics. Its mathematical model takes into account the opening (peel) displacement, coupled with tangential sliding (shear), to calculate the damage in the interfaces.

Figure 3.4 illustrates the rigidity behavior of the material as a function of the opening normalized displacement, and the evolution of the scalar damage variable as a function of the opening. The variables δ_c, δ and σ_{max} represent the characteristic strain, the ratio opening displacement/element thickness and the maximum cohesive stress, respectively.

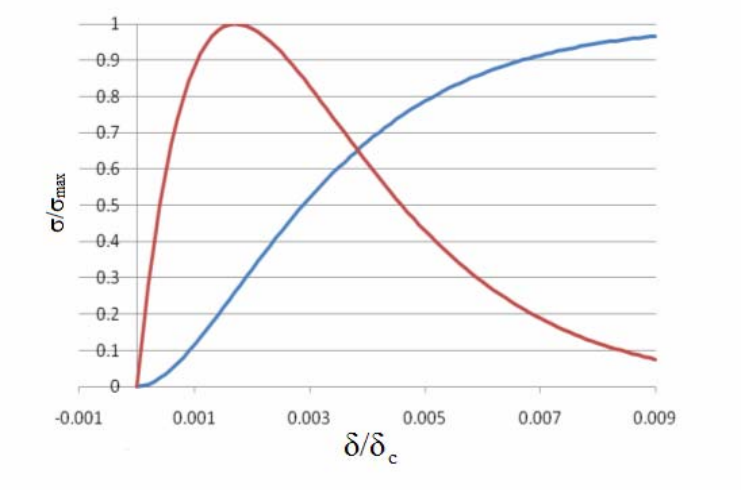

Figure 3.4. Behavior of the interface law of Smith-Ferrante: the red curve represents the ratio σ/σ_{max} and the blue curve represents the evolution of the variable scalar damage with the growth of the opening displacement.

The opening displacement δ is calculated coupled with a shear deformation, δ/δ_c coupling sliding and peeling, as follows, according to the software documentation:

$$\delta = \sqrt{\beta^2\left(\delta_{s1}^2 + \delta_{s2}^2\right) + \delta_n^2} \tag{1}$$

where δ_{s1} and δ_{s2} are the tangential sliding terms, δ_n is the normal opening of the element and β is a coupling factor. The cohesive tractions are then obtained from the opening strain energy.

During loading, the traction increases until the critical opening is reached. For higher effective openings, the cohesive forces begin to strongly decrease following an exponential curve, and delamination occurs. The law is irreversible, and the unloading way is a straight line back to the origin.

3.6 –Contact conditions

The contact element that represents well the contact between the specimen and its surroundings is the flexible contact element. It is unfortunately also the most costly in terms of computational time, since the stresses have to be computed in two elements instead of one, for each degree of freedom in contact. It models contact conditions by writing contact elements between a group of nodes (slave nodes) and a group of element faces (master faces).

To mathematically treat the problem, three new degrees of freedom representing the displacement relative to the contact surface are created for the node in contact.

After the contact is “closed”, the node and the face can again part from each other. If this distance grows further than a threshold (defined by the user), the contact element is deactivated and the contact becomes once again “open”.

The contact problem consists in an optimization, using a penalty method based in Lagrange multipliers. The solution is the minimum of the potential function F for each node and face in contact.

4 – RESULTS OBTAINED AND COMPARISON WITH THE EXPERIMENTAL TESTS

4.1 – Implicit models

4.1.1 – Point trigger

The point trigger models calculation worked well until the outer plies of the plate start to contact the stabilizing assembly. None of the full-sized models converged after a simulation time of 0.9 s for the static computation and 1.1 ms for the dynamic models, which corresponds to an approximate 5 mm displacement. The nodal displacement pattern for the last converged time step in the model is shown in Fig. 4.1, together with a comparison still from its corresponding dynamic test, taken with the high speed camera.

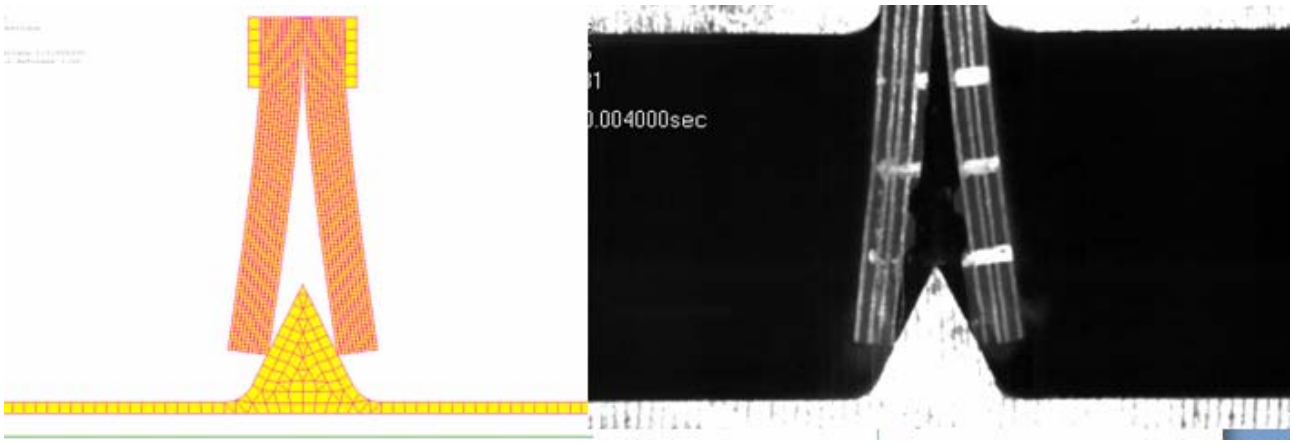

Figure 4.1. Nodal displacements for the last converged time step (left) and corresponding still frame from the test UDFoG Dynamic (right).

The crushing force was also measured as a function of the displacement of the top nodes of the plates. It was measured in two different places. First, the sum of the constraint forces on the fixed nodes of the base was computed, yielding the reaction on the impact base. Then the sum of the vertical constraint forces on the stabilizing assembly, which represented the friction force, was measured. The two were summed up and compared to the experimental results. The results that followed are shown in Fig. 4.2, for the quasi static case, where the simulation went further.

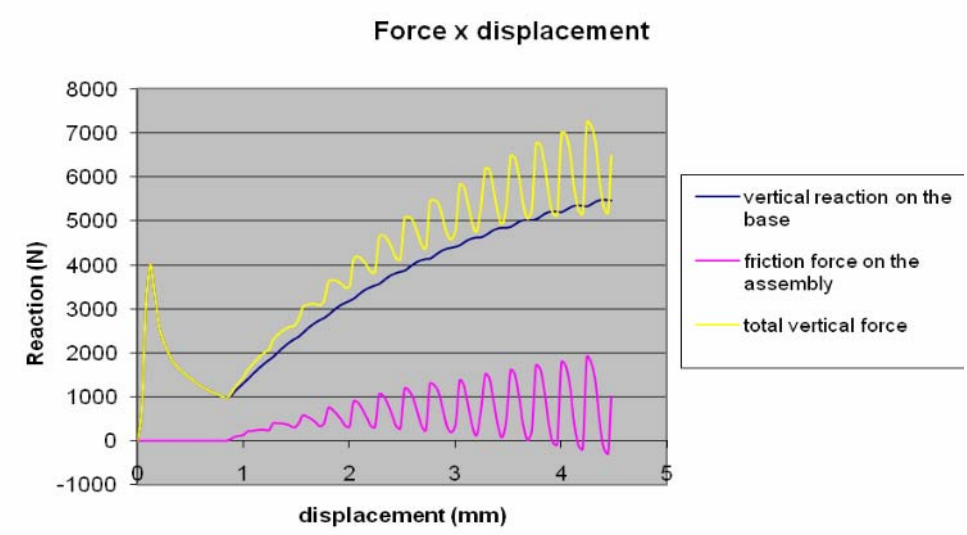

Figure 4.2. Evolution of contact forces as functions of displacements.

The behavior of the vertical reaction on the base is physically plausible and agrees with what is observed experimentally, both qualitatively and quantitatively. Initially there is a peak of force of around 4 kN, which represents the initial effort necessary to open the interfaces of the middle of the plate into two branches. After that, the branches begin to slide on the sides of the point. Since many of the middle interfaces are damaged in the first instants when the plate impacts the point, there is a sudden drop in the force. The crushing force begins to rise again due to friction, when the plate makes contact with the stabilizing assembly. The lateral kinematic constraint forces the bending of each of the two branches as whole, and the force then increases to close to 5.5 kN, when the first damages in the plies begin to appear, caused by the great compression stresses from the bending and the contact in the external plies of the structure.

The behavior of the friction forces in the lateral assembly, unfortunately, is not at all representative of the phenomenon. The presence of small oscillations in contact conditions with big sliding distances is somewhat normal due to the discretization of the structure, since the contact conditions are written in the nodes, which come in contact and leave the contact with element faces periodically. Big oscillations, however, denote a badly conditioned contact formulation. It had been already noticed in that it was the contact degrees of freedom on the region of the stabilizing assembly that had the biggest residues, and that caused the simulation to stop when it failed to achieve convergence. The analysis of the graphic confirms the problems presented by the contact conditions to the solution algorithm.

4.1.2 – Chamfer trigger

The chamfer trigger model simulations also presented convergence problems. The last converged step for a full-sized model was a little over 0.1 ms for the dynamic computation, which is equivalent to a displacement of 0.5 mm from the contact with the base. The nodal displacements for the last converged time step in the 2D model is shown in Fig. 4.3.

Figure 4.3. Nodal displacements for the last converged time step.

Once again the convergence problem presented itself in the contact degrees of freedom, and once again for the nodes of the face of the plate in contact with the stabilizing assembly.

The crushing force was once again measured as a function of the displacement of the top nodes of the plates. The results that followed are shown in Fig. 4.4, for the case where the simulation went further, which was the quasi-static one.

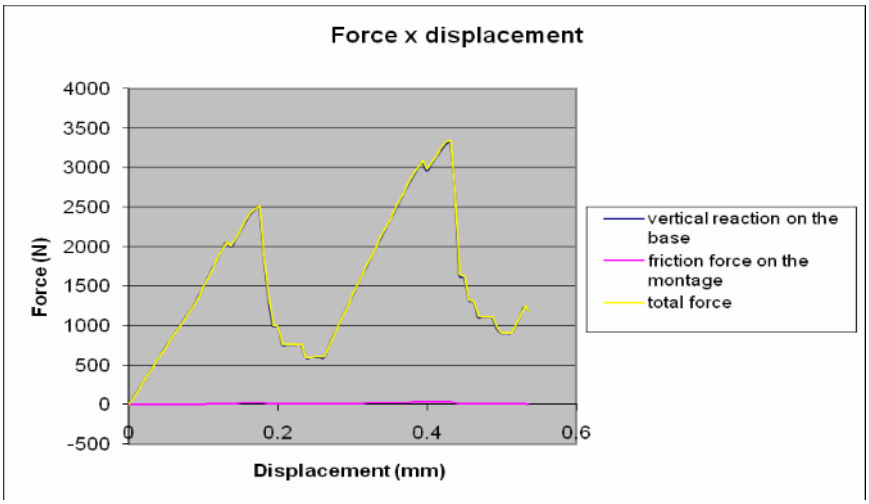

Figure 4.4. Evolution of contact forces as functions of displacement.

The force results for the chamfer trigger also agree well with the experimental results. Each of the peaks represents the force necessary to open each one of the interfaces.

4.2 – Explicit models

Unfortunately it wasn't possible, up to now, to obtain physically plausible results for the explicit solution models. All of them presented serious stability problems, especially when separation of plies occurs. In the beginning of the delamination, the node displacements start to oscillate in all directions, causing unrealistic deformations and stresses in the plies. Sometimes, as pictured in Fig. 4.5, even the contact conditions are ignored.

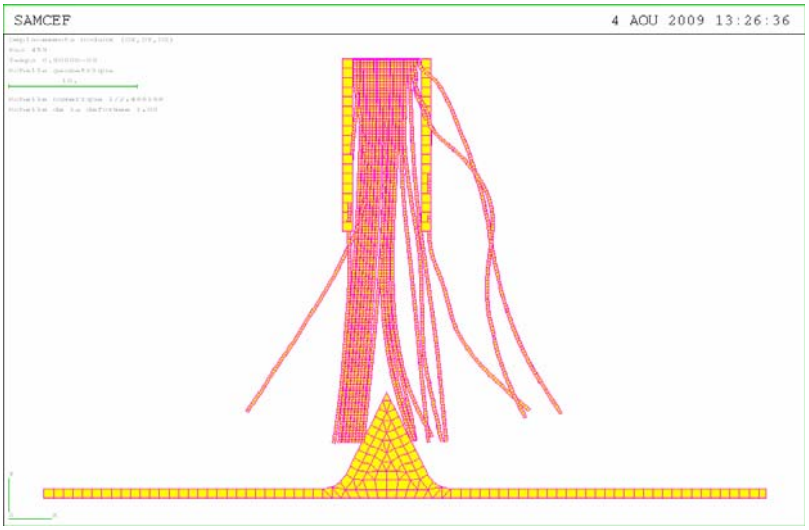

Figure 4.5. Nodal displacements for the explicit solution of the point trigger model.

The model still needs to be improved in an attempt to find solution strategies that minimize the effects of numerical instabilities.

5 – CONCLUSIONS

The model for the implicit solution showed that, as long as hypotheses definition and mathematical models for elements are concerned, it is possible to build a model that represents quite accurately the failure mechanisms present in complex phenomena such as the crush of a plate. Unfortunately, all the models, no matter which failure modes were proprietary, presented serious convergence problems, which limited the prediction of the crushing behavior only to the initiation phase.

The initiation behavior was physically coherent to the tests, which proved the capacity of the software, given the element formulations available, to model at least part of the damage behavior of the structure correctly. The contact elements, however, imposed conditions caused the simulation to stop due to lack of convergence. Reducing the time step could be a solution, but working with too small a time step in an implicit formulation problem can easily increase the solution time in a prohibitive way.

As for the explicit model, it is very promising in terms of the capacities presented by the module EUROPLEXUS, the explicit solver of the Samcef package. However, the problems due to numerical instabilities prevented us from obtaining a physically reasonable solution.

The models, then, still need much improvement in order to be robust enough to be able to fully represent the crushing phenomena of the plates, from the initiation phase until the stable phase of the crushing. Algorithms for correcting numerical instabilities have to be addressed in first place if any progress is to be made in further models. The results obtained for the present models, despite still not being complete, have been in accordance with the experimental results so far.

6. REFERENCES

Guillon, D., 2008, “Étude des mécanismes d’absorption d’énergie lors de l’écrasement progressif de structures composites à base de fibre de carbone”, Université de Toulouse, Toulouse, France.

Mamalis, A. G., Robinson, M., Manolakos, D. E., Demosthenous, G. A., Ioannidis, M. B., Carruthers, J., 1997 “Crashworthy capability of composite material structures, Composite Structures 37, pages 109-134.

Pinho, S. T., Iannucci, L., Robinson, P., 2006, “Physically based failure models and criteria for laminated fibre-reinforced composites with emphasis on fibre kinking: Part I: Development”, Composites, Part A page 37.

Samcef version 13 .html documentation, 2006, Samtech industries.

Silvestre, F. J., BUSSAMRA, F. L. S., HALD, H., 2005, Development and analysis of a ground impact attenuator for the re-entry satellite SARA. In: 18th International Congress of Mechanical Engineering, Ouro Preto. Proceedings of COBEM 2005

7. RESPONSIBILITY NOTICE

The authors are the only responsible for the printed material included in this paper.